Assessment of an Electric Vehicle Powertrain Model Based on Real-World Driving and Charging Cycles

Guanhao Du[1], *Student Member, IEEE*, Wenping Cao[1], *Senior Member, IEEE*, Shubo Hu[2], *Student Member, IEEE*, Zhengyu Lin[1], *Senior Member, IEEE*, Jing Yang[2], *Member, IEEE*, Tiejiang Yuan[2], *Member, IEEE*

[1] School of Engineering and Applied Science, Aston University, Birmingham, U.K.
[2] School of Electrical Engineering, Dalian University of Technology, Dalian, P. R. China

***Abstract*—An analytical model for an electric vehicle (EV) powertrain has been developed in this paper to study the vehicular dynamics, based on a *Nissan Leaf* EV. The electrical components of the powertrain include a battery pack, a battery management system (BMS), a DC/DC converter, a DC/AC inverter, a permanent magnet synchronous motor (PMSM), and a control system while the mechanical system consists of power transmissions, axial shaft and vehicle wheels. The driving performance of the EV is studied through the real-world driving tests and simulation tests in Matlab/Simulink. In the analytical model, the vehicular dynamics is evaluated against changes in the vehicle velocity and acceleration, state of charge (SOC) of the battery, and the motor output power. Finally, a number of EVs are introduced in the system to optimize the power dispatch. The greenhouse gas emissions of EVs are analyzed under various driving and charging conditions, and compared with conventional internal combustion engine (ICE) vehicles. For a given driving cycle, Nissan Leaf can reduce CO_2 emissions by 70%, depending on its duty cycle and the way electricity is supplied.**

Index Terms- Analytical model, electric vehicles, greenhouse gas emissions, powertrain, Nissan Leaf, V2G.

I. INTRODUCTION

CONCERNS over global warming and depleting fossil fuels have led to the rapid development of electric vehicles (EVs) to replace internal combustion engine (ICE) vehicles. Presently, major industrial countries have published their energy policies and developed economic incentives to encourage the uptake of EVs [1]-[3]. The electrical components of the EV powertrain include a battery pack, a DC/DC converter, a DC/AC converter, an electrical machine and a control system [4][5]. The pure battery EVs utilise batteries as the power source to drive the vehicle [6]. They have zero atmospheric emissions and represent a means of eco-friendly personal transportation. On the contrary, ICE vehicles and hybrid EVs employ ICE engines as the whole or part of their power source, and thus generate CO_2 emissions to some extent. The use of energy storage components can ensure a stable power supply and a quick response to the demand [7]-[9]. For example, fuel cell hybrid electric vehicles (FCHEVs) have a controllable input power from fuel cells and a supercapacitor to respond to the demand. But they are complex in control and costly in the marketplace. For instance, only 200 units of *Toyota Mirai* (FCHEV) are sold in Europe [10]. In the UK, there are 6008 charging stations for PEVs while there are only 11 hydrogen stations for FCHEVs. In terms of EV motor system, four types of electrical machines are commonly used in EVs. Compared with brushed DC motors, induction motors (IMs) and switched reluctance motors (SRMs), permanent magnet synchronous motors (PMSMs) have their advantages, such as better controllability, lighter weight, higher power density and efficiency. In this work, the EV is *Nissan Leaf* which utilizes a PMSM [11]-[13]. It is a pure EV and is one of the best-sellers in Europe. More than 300,000 cars are sold since its introduction in 2010, including 68,000 in the European market [14]. The *Nissan Leaf* powertrain includes electrical and mechanical systems. In the literature, EV powertrains are generally modeled by mechanical systems while electrical systems are overlooked [15]-[18]. In this paper, an extensive powertrain model has been built by analytical methods and Matlab/Simulink to include electrical systems.

II. SIMULATION OF EV POWERTRAIN DYNAMIC SYSTEM

A conventional EV powertrain is shown in Fig. 1. The electrical system consists of a PMSM, a battery management unit (BMU), one battery pack, a DC-DC converter and a DC-AC inverter, and an electronic controller module. The mechanical system includes a transmission system, an axle shaft and wheels train system. The vehicle speed, motor torque and speed, and battery state of charge SOC are monitored in real time. The online route and vehicle dashboard are presented in Fig. 2.

This article has been accepted for publication in a future issue of this journal, but has not been fully edited. Content may change prior to final publication. Citation information: DOI 10.1109/TVT.2018.2884812, IEEE Transactions on Vehicular Technology

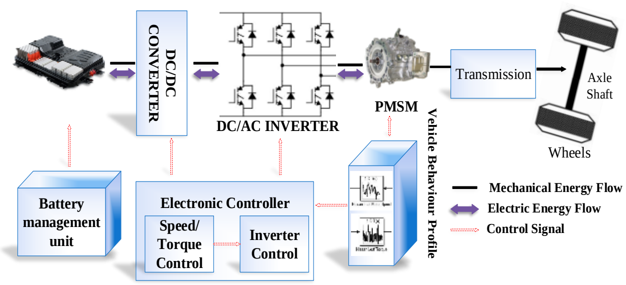

Fig. 1. The components of an EV powertrain.

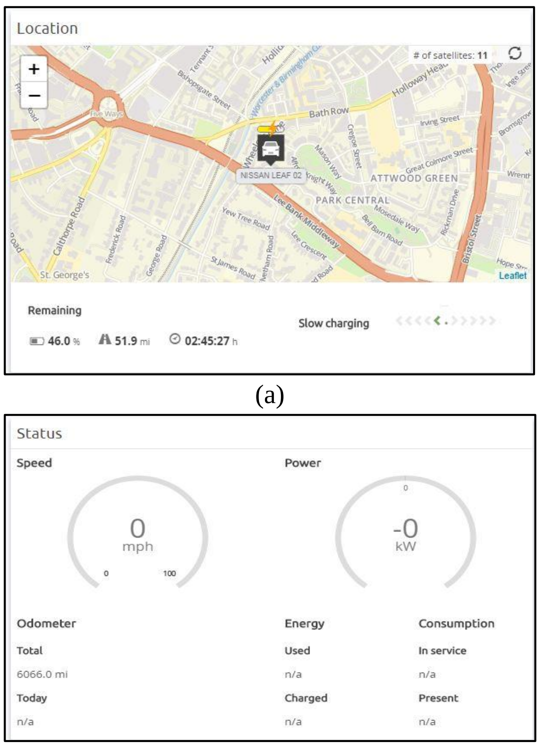

(a)

(b)

Fig. 2. Monitoring of the EV. (a) Online route. (b) Online dashboard of the Nissan Leaf EV.

A. Battery Management System (BMS)

The SOC of the battery is a key parameter as it indicates the amount of electrical energy stored in the battery. Typically, an adaptive extended Kalman filter (AEKF) is used for SOC estimation [19][20]. The Kalman filter (KF) is used to acquire the minimum mean squared error $\hat{z}_j$ of the real state z_j based on measured input and output data. It is assumed that the system is linear and measurement noise is zero-mean, independent and Gaussian noise. If the system is nonlinear, the covariance matrix of the measurement in the KF will have measurement noise. By adopting the AEKF method in the BMS, it is convenient to update the parameters in real time.

The nonlinear system model is described by:

$$z_{j+1} = f(z_j, U_j) + W_j \tag{1}$$

$$y_j = g(z_j, U_j) + v_j \tag{2}$$

where z_j is the system state vector at time index j. U_j and W_j are the measurable input and independent Gaussian noise, respectively. $f(z_j, U_j)$ is a nonlinear state transition function. y_j is the measurable output and $g(z_j, U_j)$ is the nonlinear state transition function. v_j is an independent Gaussian noise process with the statistical properties in the function.

By using an AEKF method for the BMS, the discrete function of SOC can be transferred.

$$S_{j+1} = S_j - \frac{\gamma I_k \Delta t}{C_n} \tag{3}$$

where S_j and S_{j+1} are the SOC at time j, C_n is the nominal capacity, and I_k is the current at time j. the current would be positive while discharging and negative while charging. γ is the coulombic efficiency. Normally, $\gamma = 1$ for discharging and $\gamma < 1$ for charging in standard conditions.

Assuming that $z_j = S_j$ and considering the equivalent coulombic efficiency, the state function can be derived by,

$$z_{k+1} = \begin{cases} z_k - K_{qs} - \frac{I_k \Delta t \gamma_c}{C} + w_k, & I_k < 0 \\ z_k - K_{qs} - \frac{I_k \Delta t \gamma_c \frac{\gamma_{c/3}}{\gamma_d}}{C} + w_k, & I_k > 0 \end{cases} \tag{4}$$

where γ_c and γ_d are the equivalent charge and discharge coulombic efficiency, respectively. The base coulombic efficiency in Eq. 4 is $\gamma_{c/3}$.

The combined function based on measurements is

$$y_k = g(I_k, z_k) + v_k$$
$$= K_0 - RI_k - \frac{K_1}{z_k} - K_2 z_k + K_3 \ln(z_k) + K_4 \ln(1 - z_k) + v_k \tag{5}$$

where K_0, K_1, K_2, K_3 and K_4 are the fitting coefficients, R is the internal resistance and v_k is the measurement noise.

According to Eqs. 4 and 5, a nonlinear discrete-time state space battery model is established. Therefore, the AEKF method would be adopted for estimating the SOC.

The SOC state is estimated by:

$$\hat{z}_{k/k-1} = \begin{cases} \hat{z}_{k-1/k-1} - \frac{I_k \Delta t \gamma_c}{C} + q_k, & I_k < 0 \\ \hat{z}_{k-1/k-1} - \frac{I_k \Delta t \gamma_c \frac{\gamma_{c/3}}{\gamma_d}}{C} + q_k, & I_k > 0 \end{cases} \tag{6}$$

The error covariance is:

$$P_{k/k-1} = P_{k-1/k-1} + Q_k \tag{7}$$

The Kalman gain capacitor and coefficient are:

$$\hat{C}_k = \left.\frac{\partial g(I_k, z_k)}{\partial z_k}\right|_{z_k = \hat{z}_{\frac{k}{k-1}}} = \frac{K_1}{(\hat{z}_{k/k-1})^2} - K_2 + \frac{K_3}{\hat{z}_{k/k-1}} - \frac{K_4}{1 - \hat{z}_{k/k-1}} \tag{8}$$

$$K_k = P_{k/k-1} \hat{C}_k^T [\hat{C}_k P_{k/k-1} \hat{C}_k^T + R_k]^{-1} \tag{9}$$

The measured SOC state is given by:

$$\tilde{z}_k = \ddot{z}_k - g(\hat{z}_{k/k-1}, U_k) - r_k \tag{10}$$

$$\hat{z}_{k/k} = \hat{z}_{k/k-1} + K_k \tilde{z}_k = S_{ck} \tag{11}$$

The error covariance measurement is:

$$P_{k/k} = (I - K_k \tilde{C}_k) P_{k/k-1} \tag{12}$$

B. Configuration of the EV Battery Pack

The structure of an EV battery pack is presented in Fig. 3. Two battery cells are connected in series and then in parallel with other two cells to forms a battery module. 48 battery modules are connected in series to form a battery pack. The electrical characteristics of battery cells are given in Table I. The cell voltage is rated at 3.75 V but can reach 4.2 V. The battery pack is arranged into 3 sections. One section contains 24 modules in the center of the pack. Two other sections of 12 modules each are connected in series with the central section on the two sides. The battery pack voltage is rated at 360V and its capacity is 24 kWh.

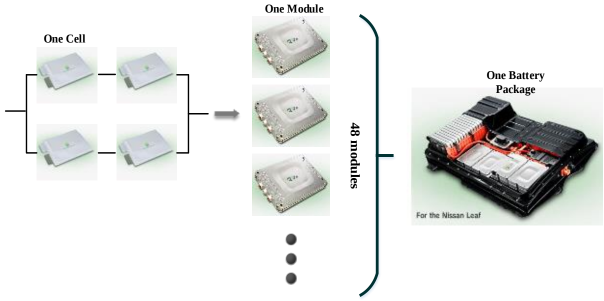

Fig. 3. The structure of an EV battery pack.

TABLE I CHARACTERISTICS OF THE NISSAN LEAF BATTERY CELLS

Cell type	Laminate type
Cathode active material	LiMn2O4 with LiNiO2
Capacity	32.5 Ah
Nominal voltage	3.75 V
Exterior dimensions	290×216 mm (L×W)
Energy density	317 Wh/L, 157 Wh/kg

C. PMSM Model Development

In the EV powertrain, a high-efficiency PMSM is used and is powered by the battery pack through a three-phase DC-AC inverter [21]. The state space equations of a PMSM in the synchronous *d*-*q* reference frame are presented by

$$\begin{cases} \frac{di_d}{dt} = \frac{1}{L_s}[U_d - R_s i_d - \omega_r L_s i_q] \\ \frac{di_q}{dt} = \frac{1}{L_s}[U_q - R_s i_q - \omega_r L_s i_d - \omega_r \varphi_{rf}] \end{cases} \tag{13}$$

where R_s and L_s are the stator-phase resistance and inductance, respectively. i_d and i_q are the *d*- and *q*-axis stator currents, and ω_r is the rotor electrical speed, respectively. U_d and U_q are the stator voltages in the *d*-*q* reference frame, and φ_{rf} is the rotor flux generated by the permanent magnets, respectively.

A discrete-time model is applied for calculating the *d*-*q* reference currents in a sampling period in the vector control. By utilising a small sampling interval, the PMSM can be modeled in a discrete time, which is called Forward Euler discretization. The expression of the discrete-time equivalent equation is given by:

$$\begin{cases} i_d(j+1) = i_d(j) + \frac{T_s}{L_s}[U_d(j) - R_s i_d(j) + E_d(j)] \\ i_q(j+1) = i_q(j) + \frac{T_s}{L_s}[U_q(j) - R_s i_q(j) + E_q(j)] \end{cases} \tag{14}$$

$$\begin{cases} E_d(j) = \omega_r(j) L_s i_q(j) \\ E_q(j) = \omega_r(j) L_s i_d(j) - \omega_r(j)\varphi_f \end{cases} \tag{15}$$

where $E_d(j)$ and $E_q(j)$ are the *d*- and *q*-axis back electromotive force (EMF) at the *j*th sampling instant; $i_d(j)$ and $i_q(j)$ are the *d*- and *q*-axis state currents at the *j*th sampling instant; $U_d(j)$ and $U_q(j)$ are the *d*- and *q*-axis state voltages at the *j*th sampling instant; $i_d(j+1)$ and $i_q(j+1)$ are the *d*-and *q*-axis state currents at the (*j*+1)th sampling instant; $U_d(j)$ and $U_q(j)$ are the *d*- and *q*-axis state voltages at the *j*th sampling instant, T_s is the sampling period in the discrete-time model, respectively. The specifications of the PMSM are presented in Table II.

TABLE II CHARACTERISTICS OF NISSAN LEAF ELECTRICAL MOTOR

Parameter	Value
Rated power	80 kW
Peak torque	280 Nm
Peak speed	10,390 rpm
Mass	56 kg
Volume	19 L
Stator O.D.	19.8 cm
Rotor O.D.	13.0 cm
Rotor pole	8
Stator slot	48
Motor efficiency	96%

Vector control is widely used in the AC drives through a space vector pulse width modulation (SVPWM) technique. A typical configuration of vector control is shown in Fig. 4 [22]. The principle is to control the *d*-axis and *q*-axis currents of the motor as per the requirements of the powertrain. This is achieved through an inner control loop (current control) and an outer control loop (speed control), both utilising a PI regulator.

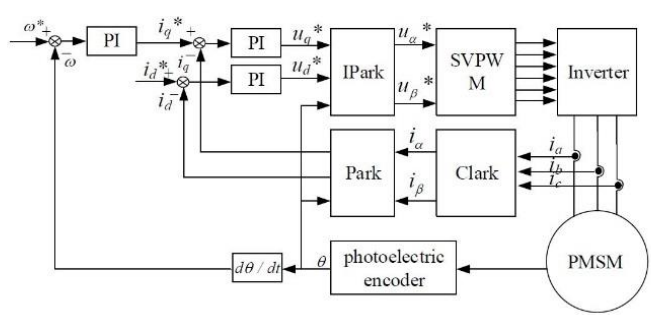

Fig. 4. Configuration of the vector control strategy.

D. Vehicle dynamic model

A vehicle dynamic model is shown in Fig. 5. According to the conventional mechanical system, the vehicle traction force F_T with a friction force between the tyre and the road surface can be expressed as

$$F_T = \frac{T_w}{r_w} - \frac{\delta_w \omega_w}{r_w} = \frac{(\sum G\gamma)T_m - \delta_{it}\omega_m}{r_w} \tag{16}$$

$$\begin{cases} \omega_w = \frac{T_w + r_w{}^2 m \omega_w \tau}{\delta_w + r_w{}^2 m(1-\tau)} \\ \tau = \frac{v_w - v_T}{\max(v_w, v_T)} \\ \delta_{it} = \delta_{it}{}^* + \frac{\delta_w}{\sum G} \end{cases} \tag{17}$$

where T_w , T_m , r_w and ω_w are the of the wheel torque, electromechanical torque, effective radius and angular acceleration of the wheels; δ_w and δ_{it} are the wheels inertia and the total inertia; G , γ , τ and m are the gear ratio, transmission efficiency, slip ratio and effective vehicle mass; v_T and v_w are the vehicle speed and wheel speed, respectively.

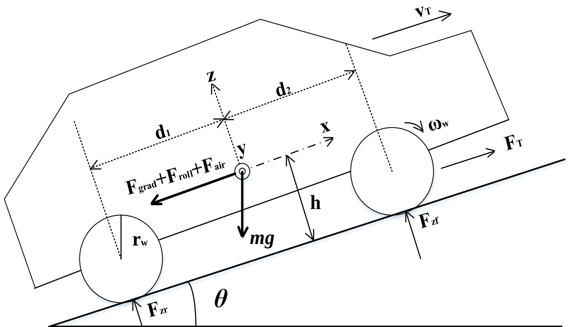

Fig. 5. The vehicle model based on the two drive wheels.

In Fig. 5, d_1 and d_2 are the horizontal distances from the front and the rear wheels to the center of gravity of the vehicle. h is the vertical distance from the center of gravity to the road surface. The vertical force (F_{zf}, F_{zr}) of the front and rear wheels in this two-wheel model can be expressed by:

$$\begin{cases} F_{zf} = \frac{d_2 \text{mgcos}\,\theta - \text{h}\left(\frac{(\sum G\gamma)T_m - \delta_{it}\omega_m}{r_w}\right)}{d} \\ F_{zr} = \frac{d_1 \text{mgcos}\,\theta + \text{h}\left(\frac{(\sum G\gamma)T_m - \delta_{it}\omega_m}{r_w}\right)}{d} \\ d = d_1 + d_2 \end{cases} \tag{18}$$

where θ , ω_m and d are the road angle, the motor acceleration, and the distance from the center to the front wheel (d_1) to the rear wheel (d_2), respectively.

From Fig. 5, the driving resistance is made up by the gradient resistance F_{grad} on the road surface, the rolling resistance F_{roll} generated by friction, and the aerodynamic resistance F_{air} caused by air friction. Therefore, the resulting traction driving force $\dot{F_T}$ can be calculated by,

$$\begin{aligned} \dot{F_T} &= F_T - (F_{grad} + F_{roll} + F_{air}) \\ &= F_T - (mg\sin\theta + \epsilon_T mg + 0.5\partial_d \rho A_T v_T{}^2) \end{aligned} \tag{19}$$

where ϵ_T, ∂_d, ρ and A_T are the coefficients of the rolling resistance and aerodynamic drag, density of air, and the front area of the vehicle, respectively.

E. Power optimisation model

The total electrical power demand can be obtained by:

$$P_{total}(i) = P_{EV}(i) + P_L(i) \tag{20}$$

where $P_{EV}(i)$ is the total EV power at time i, and $P_L(i)$ is the load power at time i.

In order to minimize the difference between the actual power demand and the mean value of the power demand, an optimisation model is required.

$$\begin{aligned} \min Z(P_{total}) &= {}^1/_{N_d} \sum_{h=1}^{N_d} (P_{total}(i) - \bar{P}_{mean})^2 \\ &= {}^1/_{N_d} \sum_{h=1}^{N_d} P_{total}(i)^2 - {}^1/_{N_d} \sum_{h=1}^{N_d} \bar{P}_{mean}{}^2 \end{aligned} \tag{21}$$

where $\bar{P}_{mean}$ is the mean power demand.

Assuming n_a and n_b are the number of batteries in different EVs employed for charging (EV1) and discharging (EV2) purposes. The power demand for flexible charging and discharging can be expressed by:

$$\begin{cases} P_{EV1} = \sum_{i=1}^{n_a} \sum_{j=1}^{N_d} P_j \times \varphi(P_{cj}, h) \times (1 - \mathrm{G_{ODT}}); \\ \quad n_a \le N_B; P_{load} \le \bar{P}_{mean} \\ P_{EV2} = \sum_{i=1}^{n_b} \sum_{j=1}^{N_d} P_j \times \varphi(P_{dcj}, h) \times (1 - \mathrm{G_{ODT}}); \\ \quad n_b \le N_B; P_{load} \ge \bar{P}_{mean} \end{cases} \tag{22}$$

$$P_{EV} = P_{EV1} - P_{EV2};\ n_V = n_a + n_b \tag{23}$$

where $\varphi(P_{cj}, h)$ and $\varphi(P_{dcj}, h)$ are the probability of a battery charging or discharging at time h, respectively. $\mathrm{G_{ODT}}$ is the probability of vehicles on the road. n_V is the total number of EVs.

By substituting Eqs. 22 and 23 into 21, the minimization problem can be developed as,

$$\begin{aligned} min\ Z &= \sum_{h=1}^{N_d} (P_{EV}(h) + P_L(h))^2 \\ &= \sum_{h=1}^{N_d} \Big(n_a \sum_{j=1}^{N_d} P_j \times \varphi(P_{cj}, h) \times (1 - \mathrm{GODT}) - \\ &\quad n_b \sum_{j=1}^{N_d} P_j \times \varphi(P_{dcj}, h) \times (1 - \mathrm{GODT}) + P_L(h) \Big)^2 \end{aligned}$$

$$\text{Subject to} \quad \begin{cases} \sum f(h) + \sum q(h) = 1 \\ f(h) \ge 0, q(h) \ge 0, \forall t \in [1, N_d] \end{cases} \tag{24}$$

where Z is the object function with respect to the optimization problem. $f(h)$ and $q(h)$ are the probability of EVs charging/discharging actions at time h. Based on these calculations, EV performance can be evaluated using the real-world operating data.

III. TEST RESULTS BASED ON REAL-WORLD DRIVING AND CHARGING CYCLES

The developed powertrain model is verified by real-world operating data.

A. Energy consumption under a daily driving cycle

The test is based on one day operation (06/10/2017) of *Nissan Leaf* in Birmingham and its route is shown in Fig. 6.

This article has been accepted for publication in a future issue of this journal, but has not been fully edited. Content may change prior to final publication. Citation information: DOI 10.1109/TVT.2018.2884812, IEEE Transactions on Vehicular Technology

Fig. 6. The driving route of the EV.

The EV started from point A to B during the period 12:48-13:00, and then went back to A from 13:25 to 13:40. Then it stopped at point C between 18:05 and 18:15. By removing the rest time, the total driving period on the day is presented in Fig. 7(a) with a condensed operating period of 32 minutes. The waveform of the motor torque and acceleration are illustrated in Fig. 7(b) and (c), receptively. During the driving period, the vehicle speed ranges from 0 to 53 mph and the acceleration is generally less than 4m/s^2, reflecting the road condition in urban Birmingham. The simulation results are presented in Figs. 8-11.

Fig. 8 shows the battery SOC results from simulation model and real tests. The red solid line represents the real test SOC and its tendency is shown in green dash line. The SOC results from the simulation model is presented in solid black. The two curves agree well with each other.

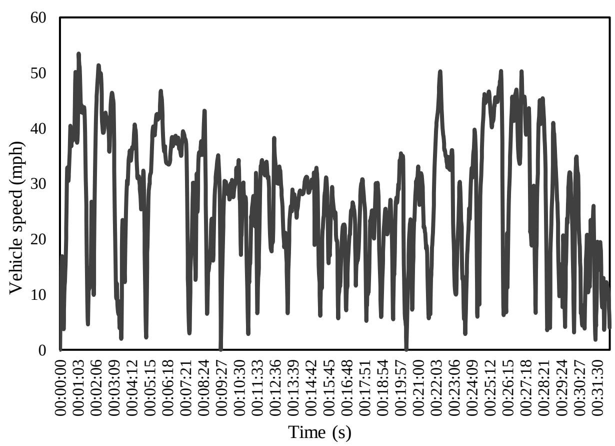

(a)

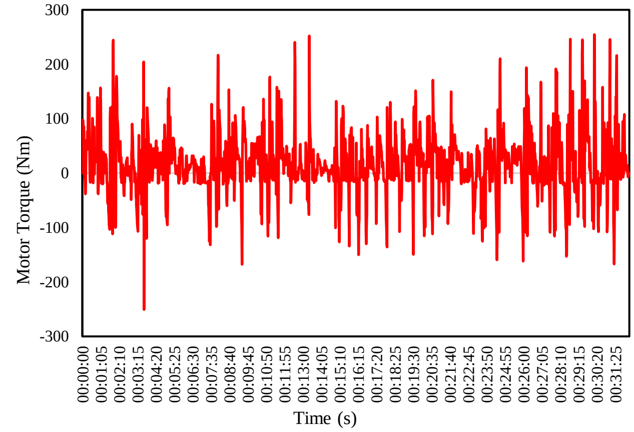

(b)

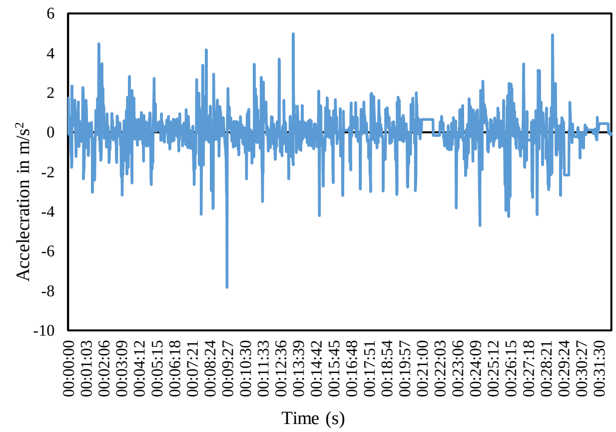

(c)

Fig. 7. EV performance. (a) Vehicle speed. (b) Motor torque. (c). The acceleration of the EV.

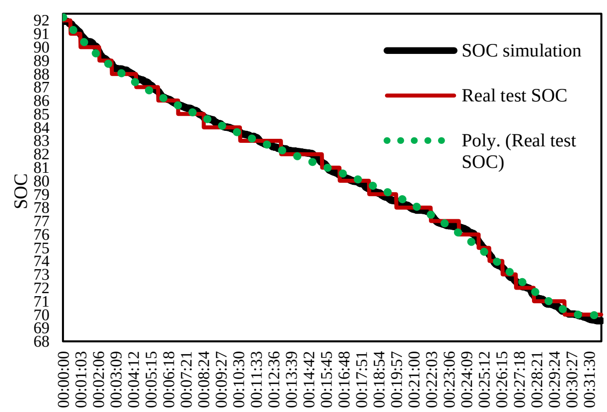

Fig. 8. Comparison of battery SOC between simulation and real tests.

This article has been accepted for publication in a future issue of this journal, but has not been fully edited. Content may change prior to final publication. Citation information: DOI 10.1109/TVT.2018.2884812, IEEE Transactions on Vehicular Technology

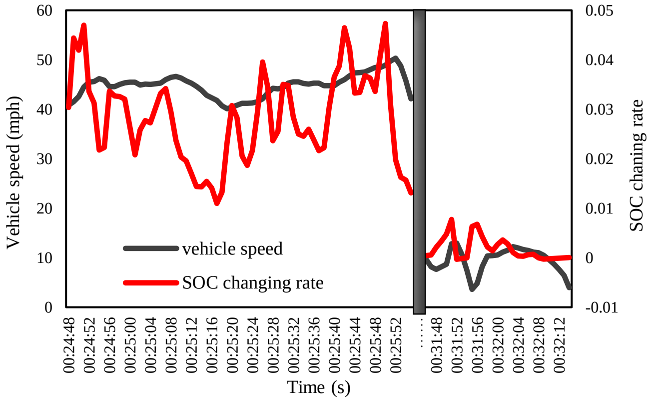

Fig. 9. Waveforms of vehicle speed and SOC changing rate.

Fig. 9 demonstrates a relationship between the vehicle speed and battery SOC. The dark solid line indicates the vehicle speed and the red line shows the changing rate of SOC. The average changing rate of SOC is around 0.03. By comparison, the SOC is under 0.008 during the period 00:31:47 to 00:32:14 in the low speed range. It is clear that the energy consumption increases with the vehicle speed. Fig. 10 further confirms the agreement between the battery SOC and energy consumption.

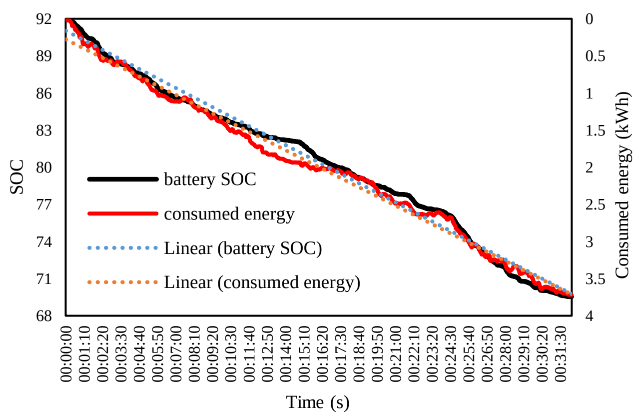

Fig. 10. The relationship between the battery SOC and energy consumption.

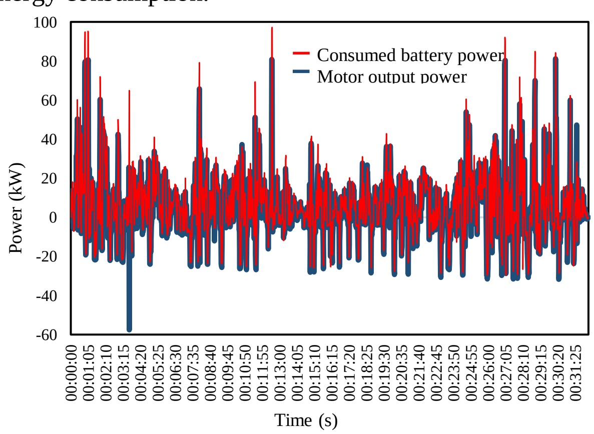

(a)

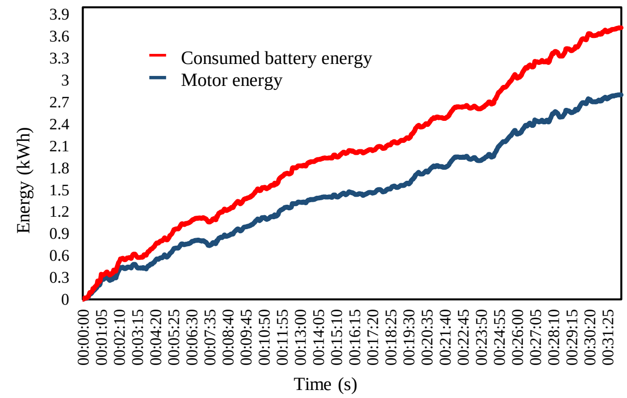

(b)

Fig. 11. Comparison of consumed power and energy. (a). Waveforms of motor power and battery power. (b). Waveforms of motor energy and battery energy.

Fig. 11(a) presents the motor power and consumed battery power during the driving cycle. Both waveforms present the similar fluctuations as the battery is the only power source. More specifically, Fig. 11(b) illustrates a comparison of energy delivered by the motor (red solid line) and the battery (blue solid line). The gap between the two is the energy lost in the transmission from the batteries to the motor.

The consumed motor energy and battery energy are given by,

$$E_{mtotal} = \sum P_m = 2.802\ kWh$$
$$E_{btotal} = \sum P_b = 3.718\ kWh$$
$$\eta = {E_{mtotal}}/{E_{btotal}} = 75.4\% \qquad (25)$$

where E_{mtotal} is the consumed motor energy, E_{btotal} is the consumed battery energy, P_m is the motor output power, P_b is the battery power and η is the energy efficiency. The efficiency (75.4%) is much better than that for conventional ICE vehicles (approximately 15%), suggesting the benefits of adopting EVs in addition to reduced CO_2 emissions.

This EV journal consumes 3.718 kWh for a distance of 27.36 km. The equivalent CO_2 emissions are calculated [23][24] in order to compare between the EV and ICE vehicles, and between different electricity generation technologies. These are tabulated in Table III based on a compact ICE car *Volswagen Golf 2012* [23]. It is clear that the use of EVs can significantly reduce the CO_2 emissions for personal transportation but they are not emission-free. Depending on how electricity is generated, this EV journal would emit equivalent CO_2 of 0.015-1.956 kg. Hydro power is the lowest as it is renewable and low in cost.

Furthermore, an annual consumption is estimated on the same journal for 200 working days per year, as shown in Fig. 12. The amount of CO_2 emissions produced by the EV are no more than 30% of an ICE vehicle. Combined with electricity generation from renewable energy, the environmental benefits of using EVs are significant.

This article has been accepted for publication in a future issue of this journal, but has not been fully edited. Content may change prior to final publication. Citation information: DOI 10.1109/TVT.2018.2884812, IEEE Transactions on Vehicular Technology

TABLE III COMPARIOSN OF CO_2 EMMISSIONS

Type of vehicles	Electricity source	CO_2 (kg)
ICE	--	6.68
EV	Conventional fuel	1.96
	Mixed (fuel and renewable)	1.32
	Solar	0.26
	Wind	0.045
	Hydro	0.015

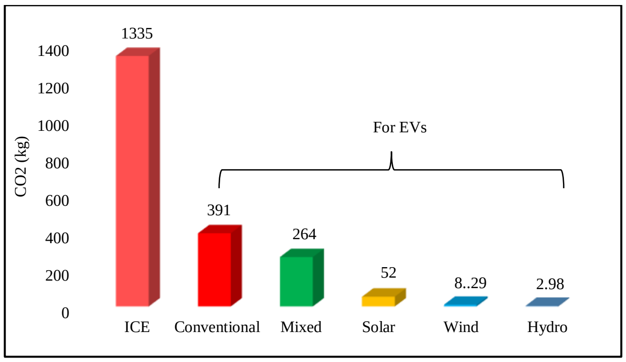

(b)

Fig. 12. Comparison of annual CO_2 emissions.

B. Power dispatch under a daily charging cycle

In order to optimize the power dispatch, a number of similar EVs are involved based on the previous demand power, number of the vehicles, and probability of EVs connecting to the grid. The load profiles for different numbers of EVs are obtained and presented in Fig. 13.

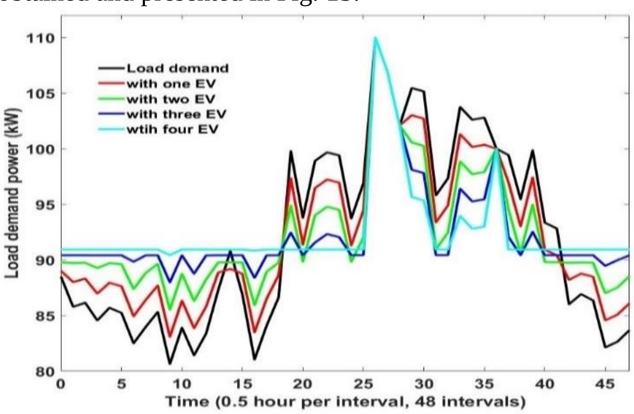

Fig. 13. Optimized and original power demand profiles.

Under this condition, the load demand in 24 hours is based on the European Bioenergy Research Institute (EBRI) building in Birmingham, which is equipped with several charging stations for *Nissan Leaf*. Among these is one vehicle-to-grid (V2G) charging station, which is used in this study. The demand is obtained in 48 intervals (0.5 hour each). The EV's V2G performance is evaluated according to the different number of EVs (1-4) connected to the grid. The probability of EV connecting to the power system network is derived from the rest time in the previous EV journal. In order to keep the EV operational for daily travels, the maximum energy for V2G operation is limited. In this case, it is 70% of capacity which can be used for V2G grid support. From Fig. 13, the fluctuations of load demand are minimized by increasing the number of EVs for flexible charging and discharging operation. The optimized load demand would be much closer to the idealized mean load. However, as the EVs do not support the power network during driving periods, some fluctuations are not minimized in the figure.

IV. CONCLUSIONS

In this paper, an analytical model of an EV powertrain has been presented, including both mechanical and electrical sub-systems. The system dynamic responses to changes in vehicle speed, acceleration, machine speed and torque have been studied in detail. An online AEKF SOC method is developed for battery management. The analytical model of the EV powertrain has been validated by simulation and actual test results from the test driving cycles. EV power and energy consumption based on the real driving tests can also be obtained to estimate their impact on the environments. Finally, a flexible power dispatch can be achieved by utilizing more EVs under controlled charging and discharging conditions. Therefore, EVs can be scheduled to support the power grid through V2G operation.

REFERENCES

[1] U. R. Prasanna and A. K. Rathore, "Dual three-pulse-modulation (DTPM) based high-frequency pulsating DC link two-stage three-phase inverter for electric/hybrid/fuel cell vehicles applications," *IEEE J. Emerg. Sel. Topics Power Electron.*, vol. 2, no. 3, pp. 477-486, Sep. 2014.

[2] B. Zhou and T. Litter, "Local storage meets local demand: a technical solution to future power distribution system," *IET Generation, Transmission & Distribution*, vol. 10, pp. 704-711, Feb. 2016.

[3] K. Rajashekara, "Present status and future trends in electric vehicle propulsion technologies," *IEEE J. Emerg. Sel. Topics Power Electron.*., vol. 1, no. 1, pp. 3-10, Mar. 2013.

[4] C. M. Lai, Y. H. Cheng, M. H. Hsieh and Y. C. Lin, "Development of a bidirectional DC/DC converter with dual-battery energy storage for hybrid electric vehicle system," *IEEE Trans. Veh. Technol.*, vol. 67, no. 2, pp. 1036-1052, Feb. 2018.

[5] S. Akhegaonkar, L. Nouveliere, S. Glaser and F. Holzmann, "Smart and green ACC: energy and safety optimization strategies for EVs," *IEEE Trans. on Systems, Man, and Cybernetics: Systems*, vol. 48, no. 1, pp. 142-153, Sep. 2016.

[6] H. A. Yavasoglu, J. Shen, C. Shi, M. Gokasan and A. Khaligh, "Power split control strategy for an EV

powertrain with two propulsion machines," *IEEE Trans. on Transportation Electrification*, vol. 1, no. 4, pp. 382-390, Dec. 2015.

[7] D. Zhou, A. A. Durra, I. Matraji, A. Ravey and F. Gao, "Online energy management strategy of fuel cell hybrid electric vehicles: a fractional-order extremum seeking method," *IEEE Trans. Ind. Electro.*, vol. 65, pp. 6787-6799, Aug. 2018.

[8] H. S. Das, C. W. Tan and A. H. M. Yatim, "Fuel cell hybrid electric vehicles: A review on power conditioning units and topologies," *Renewable and Sustainable Energy Reviews*, vol. 76, pp. 268-291, Sep. 2017.

[9] H. Fathabadi, "Fuel cell hybrid electric vehicle (FCHEV): Novel fuel cell/SC hybrid power generation system," *Energy Conversion and Management*, vol. 156, pp. 192-201, Jan. 2018.

[10] TOYOTA Global Newsroom. Toyota sells 1.52 million electrified vehicles in 2017, three years ahead of 2020 target [Online]. Available: https://newsroom.toyota.co.jp/en/corporate/20966057.html?adid=ag478_mail&padid=ag478_mail

[11] J. D. Widmer, R. Martin and M. Kimiabeigi, "Electric vehicle traction motors without rare earth magnets," *Sustainable Materials and Technologies*, vol. 3, pp. 7-13, Apr. 2015.

[12] J. Santiago, H. Bernhoff, B. Ekergard, S. Eriksson, S. Ferhatovic, R. Waters, and M. Leijon, "Electrical motor drivelines in commercial all-electric vehicles: a review," *IEEE Trans. Veh. Technol*, vol. 61, no. 2, pp. 475-484, Feb. 2012.

[13] H. Busch, M. Duoba, E. Rask and M. Meyer, "Advanced powertrain research facility AVTA Nissan leaf testing and analysis," *Energy Efficiency and Renewable Energy*, 2012.

[14] Nissan Official Newsroom. Nissan delivers 300,000th Nissan Leaf [Online]. Available: http://nissannews.com/en-US/nissan/usa/channels/us-united-states-nissan/releases/nissan-delivers-300-000th-nissan-leaf

[15] X. Y. Zhou, D. T. Qin and J. J. Hu, "Multi-objective optimization design and performance evaluation for plug-in hybrid electric vehicle powertrains," *Applied Energy*, vol. 208, pp. 1608-1625, Dec. 2017.

[16] E. A. Grunditz and T. Thiringer, "Characterizing BEV powertrain energy consumption, efficiency, and range during official and drive cycles from Gothenburg, Sweden," *IEEE Trans. Veh. Technol.*, vol. 65, no. 6, pp. 3964-3980, Jun. 2016.

[17] F. L. Mapelli, D. Tarsitano and M. Mauri, "Plug-in hybrid vehicle: modeling, prototype realization, and inverter losses reduction analysis," *IEEE Trans. Ind. Electro.*, vol. 57, pp. 598-607, 2010.

[18] A. Nair and K. R. Rajagopal, "Generic model of an electric vehicle for dynamic simulation and performance prediction," *Electrical Machines and Systems 2010 International Conf.*, pp. 753-757, 2010.

[19] J. Wang, J. Guo and D. Lei, "An adaptive Kalman filtering based state of charge combined estimator for electric vehicle battery pack," *Energy Conversion and Management*, Vol. 50, pp. 3182-3186, 2009.

[20] J. F. Yang, B. Xia, Y. L. Shang, W. X. Huang and C. C. Mi, "Adaptive state-of-charge estimation based on a split battery model for electric vehicle applications," *IEEE Trans. Veh. Technol.*, vol. 66, no. 12, pp. 10889-10898, Dec. 2017.

[21] C. Shi, Y. C. Tang and A. Khaligh, "A single-phase integrated onboard battery charger using propulsion system for plug-in electric vehicles," *IEEE Trans. Veh. Technol.*, Vol. 66, no. 12, pp. 10899-10910, Dec. 2017.

[22] F. L. Zhang, X. L. Wang, Q. X. Liao and C. Gu, "Highly integrated bidirectional vehicle to grid (V2G) for electric vehicles based on open winding permanent magnet synchronous motor," *IEEE International Conference on Electrical Machines and Systems (ICEMS)*, Oct. 2017.

[23] E. Pike, "Calculating electric drive vehicle greenhouse gas emissions," *International Council on Clean Transportation (ICCT)*, Aug. 2012.

[24] "New car CO_2 report 2017, the 16th edition," *The Society of Motor Manufacturers and Traders Ltd.*, 2017.

Guanhao Du (S'14) received the B.Eng degree in electrical engineering and automation from Soochow University, Suzhou, China, and the M.Sc degree in electrical power engineering from Newcastle University, Newcastle, UK, in 2013 and 2014, respectively. He is currently working toward the PhD degree in smart grids at Aston University, Birmingham, UK.

Wenping Cao (M'05-SM'11) received the B.Eng in electrical engineering from Beijing Jiaotong University, Beijing, China, in 1991, and the Ph.D. degree in electrical machines and drives from the University of Nottingham, Nottingham, U.K., in 2004. He is currently Chair Professor of Electrical Power Engineering and Head of Power Electronics, Machines and Power System (PEMPS) Group at Aston University, Birmingham, U.K.

Shubo Hu (S'14) received the B.S. degree in electrical engineering from Dalian University of Technology, Dalian, China, in 2012. Currently, she is a doctoral candidate in school of electrical engineering, Dalian University of Technology, China.

This article has been accepted for publication in a future issue of this journal, but has not been fully edited. Content may change prior to final publication. Citation information: DOI 10.1109/TVT.2018.2884812, IEEE Transactions on Vehicular Technology

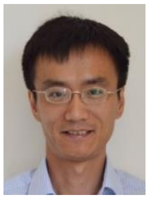

Zhengyu Lin (S'03-M'05-SM'10) received the B.Sc. and M.Sc. degrees from the College of Electrical Engineering, Zhejiang University, Hangzhou, China, in 1998 and 2001, respectively, and the Ph.D. degree from Heriot-Watt University, Edinburgh, U.K., in 2005. He is currently a Lecturer in Department of Electrical, Electronic and Power Engineering, Aston University, Birmingham, U.K.

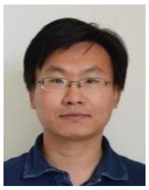

Jind Yang (S'08-M'11) received the B.E. and M.Sc. degrees from North China Electric Power University, Baoding, China, in 2003 and 2006, respectively, and the Ph.D. degree from the University of Glasgow, Glasgow, U.K., in 2011, all in electrical engineering.

Prof Tiejiang Yuan (M'11) received his MSc and PhD degrees in power systems from Xinjiang University, China, in 2009 and 2012, respectively. He is a Professor with the School of Electrical Engineering, Dalian University of Technology, China.